RSC Advances

PAPER

View Article Online
View Journal | View Issue

Cite this: *RSC Adv.*, 2021, **11**, 11952

Effect of the pore structure of an active alumina catalyst on isobutene production by dehydration of isobutanol

Kaige Tian, Qin Li, Weili Jiang, Xiaosheng Wang, Shicheng Liu, Yapeng Zhao and Guanglin Zhou*

An alumina catalyst was prepared by mixing and pinching with pseudo-boehmite, and the catalyst was reamed with polyethylene glycol. The catalysts prepared were characterized by means of XRD, mercury injection and NH_3-TPD, and the dehydration properties of the catalysts prepared with different amounts of reamer were evaluated in a 10 mL fixed bed reactor with 5% water as a raw material. The results showed that the addition of reamer did not affect the crystal structure and the amount of acid of the catalyst. With the increase of the amount of reamer, the pore volume of the catalyst increased continuously, the number of large pores increased, the conversion rate of isobutanol increased, and the selectivity of isobutene remained basically unchanged. When the amount of reamer is 30%, the isobutanol conversion rate is the best. The isobutanol conversion rate and the isobutene selectivity were 97% and 93% respectively under the conditions of 330 °C, 0.1 MPa and 12 h^{-1} air velocity of the body liquid.

Received 7th January 2021
Accepted 12th March 2021

DOI: 10.1039/d1ra00136a

rsc.li/rsc-advances

1. Introduction

Isobutylene is an important part of the petrochemical industry.[1–3] As an important organic raw material in the global chemical industry, a large amount of isobutylene is needed every year to produce other chemicals, including downstream chemicals such as MTBE,[4] polyisobutylene,[5] butyl rubber, tert-butanol, and ABS resin.[6–9] The current industrial processes for the production of isobutylene are mainly based on steam cracking and fluid catalytic cracking, which involve vast amounts of energy and significant CO_2 emissions.[10–14] The dehydration of biomass alcohol to obtain isobutylene is a more economical and environmentally friendly approach than petroleum-based systems.[15,16] The process of dehydrating biomass alcohol to olefins is relatively well-established.[17] For example, a joint venture established by Dow Chemical and Brazil's CRYSTALSEV to produce polyethylene from sugar cane has been in production for many years. Here, the main catalysts for alcohol dehydration to olefins are alumina,[18–20] heteropolyacids, transition-metal oxides,[21] and HZSM-5 molecular sieve catalysts.[22] The stability of heteropolyacid and transition metal oxide catalysts is poor, and the catalyst is easily deactivated when the temperature rises. Moreover, the selectivity of heteropolyacid catalysts becomes poor as the temperature increases. Olefins tend to aggregate, and by-products increase.[23–25] The preparation method is complicated and expensive and not conducive to industrial use.

Both HZSM-5 molecular sieve and alumina catalysts are used in the reaction of ethanol dehydration to ethylene on an industrial scale. Molecular sieves are well known for their adjustable acidity and shape-selective catalysis,[26] but they are rapidly deactivated due to coke deposition. Therefore, the preparation of thermally stable catalysts with anti-coking properties has important meaning and high value. This can be achieved through a flexible catalyst design.[27] The catalyst carrier is not only a support, but also a carrier to provide a complex microenvironment—this is a key factor in determining the catalytic function.[28] The catalyst carrier should have sufficient thermal stability to maintain the shape of the catalyst and provide an open structure for the catalyst. This can make it easy to contact the reactants and prevent the coke from clogging the pores.[29,30]

Porous alumina is one of the most widely used materials in industry. It has good structural properties and thermal stability. Unfortunately, the pore size of alumina is small, and the reactants tend to stay in the small pores leading to coking and side reactions that inevitably deactivate the catalyst.[30,31] According to reports, glucose, hydroxy acids, and urea can be used as pore formers in catalysts to change the morphology/texture of different oxide catalysts.[32–34]

Here, we studied the relationship between polyethylene glycol as a low-cost pore-forming agent and the structure and catalytic performance of alumina. We adjusted the pore structure of alumina by changing the amount of polyethylene glycol added. A series of rod-shaped porous alumina materials were

College of New Energy and Materials, China University of Petroleum-Beijing, 18, Fuxue Road, Changping District, Beijing, 102249, China. E-mail: zhouguanglin2@cup.edu.cn; Tel: +86-10-89731160

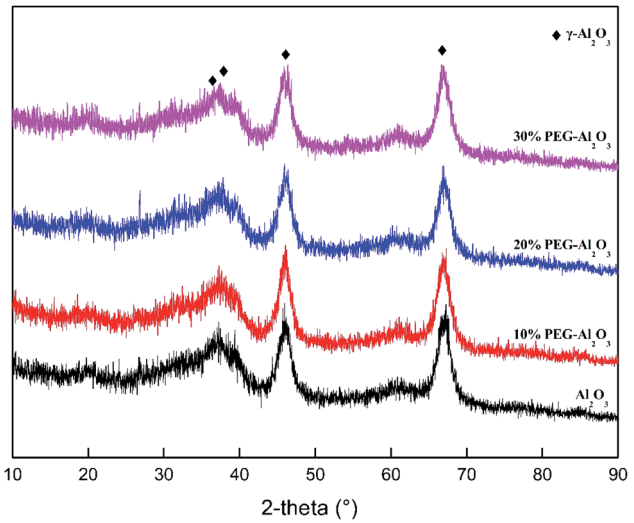

Fig. 1 XRD patterns of PEG-modified Al_2O_3 at different PEG loadings.

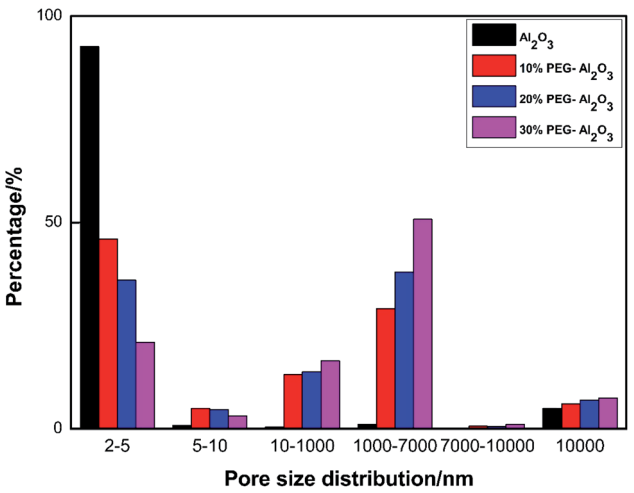

Fig. 2 Pore size distribution of PEG-modified Al_2O_3 at different PEG loadings.

prepared with the equal volume impregnation method. The modified alumina served as a catalyst for the reaction of isobutanol dehydration to prepare isobutene with higher selectivity and activity. This greatly reduces the deactivation rate.

2. Results

2.1. X-ray diffraction (XRD)

Fig. 1 shows XRD patterns of PEG-modified Al_2O_3 at different contents of PEG. A diffraction peak of γ-Al_2O_3 at $2\theta = 67.00°$, 45.84°, 39.47°, and 37.59° is observed at PEG loadings of 10 wt% or higher. This indicates that the crystal structure of the catalyst is γ-Al_2O_3 (COD: 01-079-1158).[35] The crystalline modifications of γ-Al_2O_3 were not observed; that is, the crystal structure of the catalyst with different additive contents is the same. The PEG additive does not affect the crystal structure of γ-Al_2O_3.

2.2. Automatic mercury porosimeter and the adsorption–desorption isotherms of nitrogen

The pore size distribution and physical structure data of the catalysts prepared with different amount of reamer during the preparation process are shown in Fig. 2 and Table 1, respectively. Table 1 shows the total pore volume (V_p) and the mean pore size (MPS). This changed to a higher extent for the supports obtained with different PEG contents. Table 1 shows that, upon adding the expanding agent to the catalyst, the average pore diameter is sufficiently greater than that without the expanding agent. Moreover, with increasing proportion of the added expanding agent, a significant increase in the pore volume and average pore diameter of the catalyst occurs. The pore size distribution of the expanding agent has a more significant influence on the entrance and pore diameter. This may be caused by the fact that the polymer PEG 400 has short helices and, when added during sample preparation, can aid in obtaining materials with a somewhat tight structure.[36]

As can be seen from Fig. 2, macropores were produced by the addition of reamer. With increasing proportion of reamer, the proportion of pore diameters of 2–5 nm in the prepared catalyst gradually decreased, from 92.61% to 21.02%, while the proportion of 1000–7000 nm macropores increased significantly, from 1.05% to 50.81%. The macroporous aperture ratio increased to improve the mass transfer performance of the catalyst. Upon injecting isobutanol into the hole and the living heart center of the contact reaction, the reaction of isobutylene molecules easily spreads out at the same time, reducing the secondary reaction of isobutylene, which occurs as a result of the coked catalyst deactivation, thus improving the catalytic

Table 1 Specific surface area and pore structure properties of PEG-modified Al_2O_3 at different PEG loadings

			Pore size distribution[a]/%						
Catalyst	S_{BET}[b] ($m^2\ g^{-1}$)	V_P[a] ($mL\ g^{-1}$)	2–5	5–10	10–10^3	10^3–7 × 10^3	7 × 10^3–10^4	≧10^4	MPS/nm
Al_2O_3	308.61	0.3088	92.61	0.83	0.44	1.05	0.12	4.96	4
10% PEG-Al_2O_3	239.60	0.4974	46.04	4.96	13.19	29.11	0.64	6.06	8.3
20% PEG-Al_2O_3	223.95	0.5432	36.01	4.64	13.88	37.95	0.6	6.92	11.8
30% PEG-Al_2O_3	130.24	0.6175	21.02	3.09	16.53	50.81	1.06	7.49	19

[a] MIP analysis. [b] The specific surface area of the catalyst sample was calculated with the Brunauer–Emmett–Teller (BET) method.

subject activity stability.[37] Therefore, the catalyst with reaming agent has good catalytic de-watering activity.

2.3. Thermo gravimetry-differential thermal analysis (TG-DTA)

The amount of coke formed on the spent catalysts was evaluated by TG in airflow. Fig. 3(a) shows the difference in the TG profiles between the Al_2O_3 and 30% PEG-Al_2O_3 catalysts. Two used samples were prepared by being recovered after the reaction at 330 °C for 24 h. All the used catalysts had a decrease in weight at temperatures higher than 200 °C. The difference in weight loss between the Al_2O_3 and 30% PEG-Al_2O_3 catalysts must be attributed to the carbon deposition. The carbon content, which was calculated from the difference in the TG curves between the Al_2O_3 and 30% PEG-Al_2O_3 catalysts, was 16.81 and 12.34 wt%. This result showed that the amount of coke formed over the Al_2O_3 catalyst was significantly higher than that formed over the 30% PEG-Al_2O_3 catalyst.

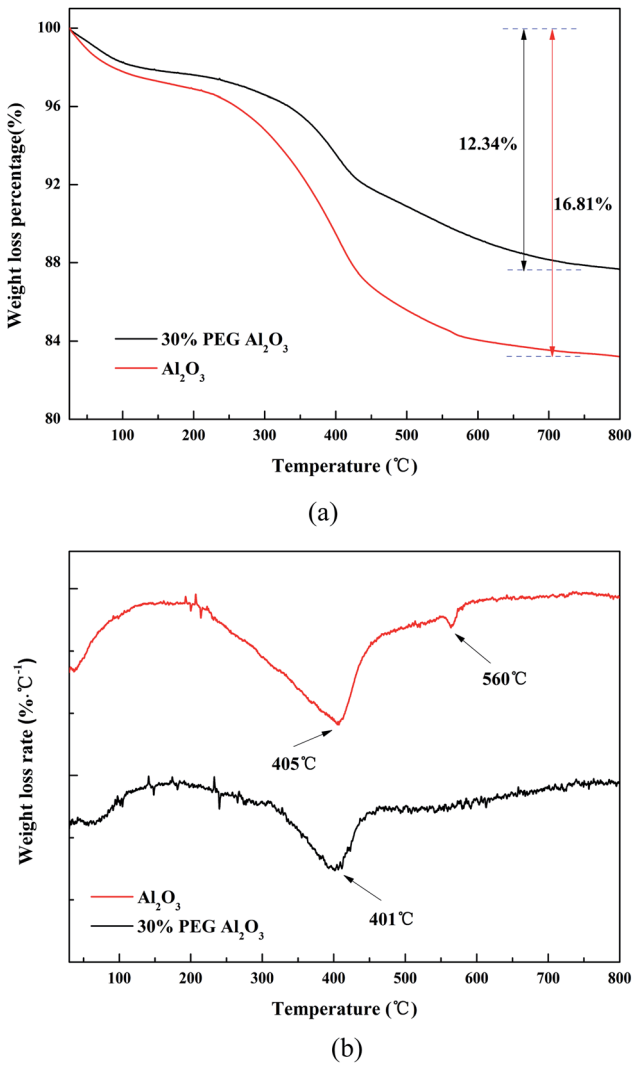

Fig. 3 Characterization of the spent catalysts after the isobutanol dehydration, after 24 hours of reaction. (a) TG-air test, and (b) DTG curves in air.

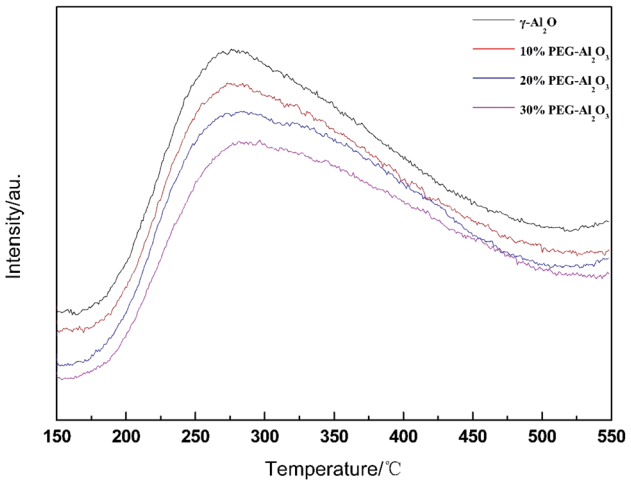

Fig. 4 NH_3-TPD of PEG-modified Al_2O_3 at different PEG loadings.

Fig. 3(b) shows the DTG curve. The DTG curve indicates that the weight losses of the spent catalysts occurred at 400 °C and 560 °C. The peak at 400 °C in the DTG curve might be related to the amorphous coke that was easily oxidized. The peak at 560 °C could be assigned to the coke with high crystallinity.[38]

Thus, it is assumed that carbon is relatively difficult to accumulate on 30% PEG-Al_2O_3 because of the large pores of 30% PEG-Al_2O_3. In other words, PEG-modified alumina exhibits the suppression of coking.

2.4. The temperature-programmed desorption of adsorbed NH_3 (NH_3-TPD)

NH_3-TPD experiments were carried out to analyze the number and strength of the acid sites. It was observed from Fig. 4 that all the samples presented a broad desorption peak ranging from 150 °C to 500 °C. The shapes of the profiles were simple and symmetric, suggesting the presence of the same acid sites. To further investigate the distribution of acid sites, the asymmetric profiles were fitted by a Gaussian function. The patterns exhibited one desorption peak, while the peak centered between 220 °C and 290 °C was assigned to the deliberation of medium-strong acid sites. The distribution of surface acidity was similar in Al_2O_3, and the fraction of the type of acid sites in the former does not show a significant change with the loading of different PEG contents. In the isobutanol dehydration reaction, higher acid content and acid strength are conducive to the dehydration reaction. However, if the acid strength is too high, side reactions, superposition, and cracking reactions will also occur.[39] Therefore, the dehydration reaction needs an appropriate acid content and strength. The amount of acid and acid strength of the four catalysts basically changed slightly. With increasing amount of reamer added, the total amount of acid in the catalyst decreased slightly, as did the amount of medium strong acid. When the amount of reamer added was 30%, the amount of medium strong acid in the catalyst was the lowest. This is

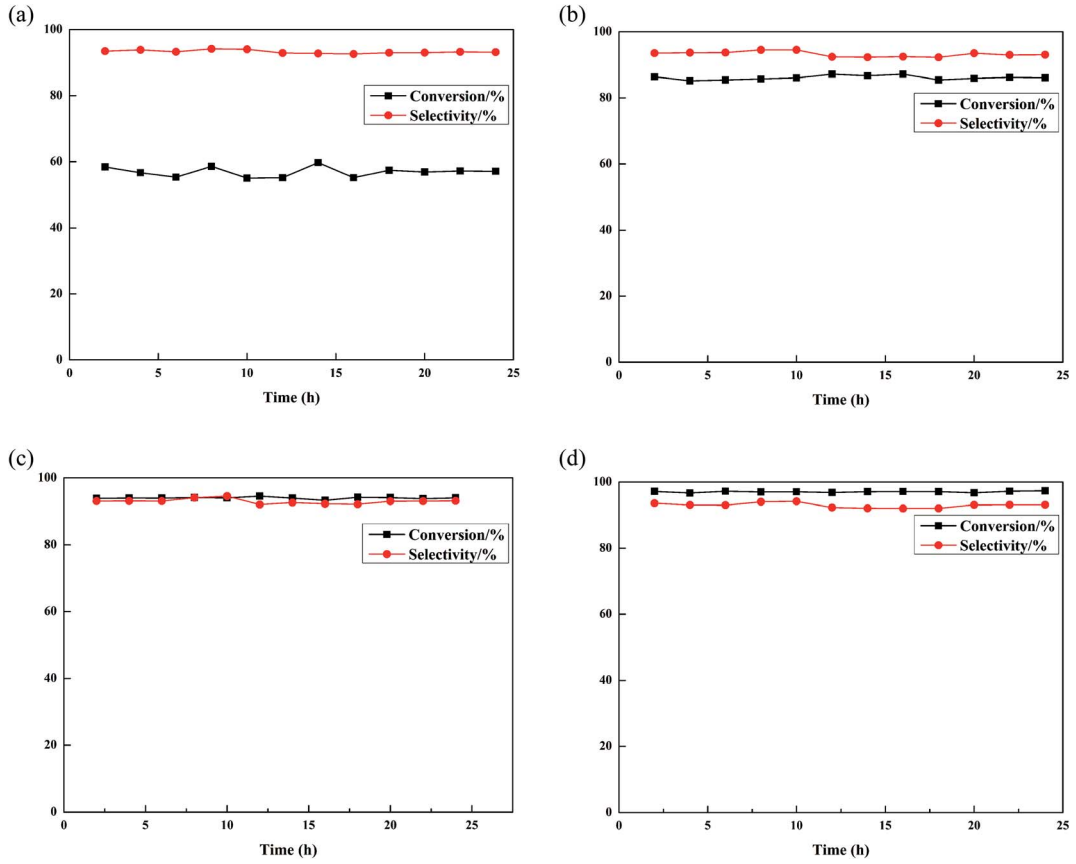

Fig. 5 Catalytic activity of PEG-modified Al_2O_3 at different PEG loadings: (a) Al_2O_3; (b) 10% PEG-Al_2O_3; (c) 20% PEG-Al_2O_3; and (d) 30% PEG-Al_2O_3.

beneficial to inhibit the occurrence of side reactions and improve selectivity.[40,41]

2.5. Catalytic activity of PEG-modified Al_2O_3 at different PEG loadings

The pressure is 0.1 MPa when the reaction temperature is 330 °C, and the volume liquid space velocity is 12 h^{-1}. The reaction performance of isobutanol dehydration to isobutene with different pore expander amounts of the γ-Al_2O_3 catalyst is shown in Fig. 5. The specific data of the main products are shown in Table 2. Under 24 h of continuous reaction conditions, the isobutanol conversion rate of the catalyst without adding the pore expander is about 57% (Fig. 5a), and the catalyst isobutanol conversion rate when the pore expander is 10% is 86%. The isobutanol conversion rate of the catalyst added with the pore expander is significantly increased and constant. The isobutanol conversion rate of the catalyst is significantly increased when 30% of the pore expander is added to the catalyst. The conversion rate of isobutanol reached 97%. The addition of the pore expander increases the pore volume and pore diameter of the catalyst. The addition of the pore expander increases the contact surface between the reactant and the active center of the catalyst. The addition of the pore expander improves the mass transfer performance of the catalyst, promotes the diffusion of raw materials and product molecules,

Table 2 Dehydration of isobutanol over PEG-modified catalysts[a]

		Selectivity[b]/%							
Catalyst	Conversion[b]/%	CH_4	C_2H_4	C_3H_6	1-C_4H_8	*cis*-2-C_4H_8	*trans*-2-C_4H_8	*iso*-C_4H_8	*tert*-C_4H_8
Al_2O_3	56.9	0.4	0.8	0.9	1.6	0.7	0.6	93.3	1.2
10% PEG-Al_2O_3	86.0	0.3	0.6	0.5	2.3	0.5	0.4	93.2	1.3
20% PEG-Al_2O_3	93.9	0.3	0.9	0.8	1.9	0.4	0.4	93	1.5
30% PEG-Al_2O_3	97.0	0.1	0.5	0.6	2	0.3	0.2	92.9	2.1

[a] Reaction conditions: $P = 0.1$ MPa; $T = 330$ °C; LHSV = 12 h^{-1}. [b] Average activity in the initial 24 h.

suppresses the occurrence of plugging and coking, and improves the conversion rate of the catalyst.[42] Therefore, there is better dehydration performance of the catalyst for isobutanol with increasing amounts of pore expander. The order of the pore size of the four catalysts from large to small is 30% pore expander >20% pore expander >10% pore expander >0% pore expander. The 30% pore expander catalyst has the largest pore size and pore volume. The 30% pore expander catalyst has the highest conversion rate of isobutanol. However, the selectivity of isobutylene did not change much during the experiment, and the selectivity of isobutylene of the four catalysts was about 93%.

2.6. Compressive strength test

The compressive strength of the catalyst is an important indicator to measure whether the catalyst can be used in a fixed bed reactor. According to the measurement results in Table 3, as the amount of PEG added continues to increase, the compressive strength of the alumina catalyst gradually decreases. This may be because, by adding PEG, the macropores in the catalyst gradually increase, making the catalyst easier to fragment under external stress conditions. However, the reduction in compressive strength is very small and can be ignored. It can still be applied to fixed-bed reactors, which means that the catalyst is easier to industrialize for application.

3. Materials and methods

3.1. Samples

The pseudo-boehmite powder and Sesbania powder were purchased from Shandong Zibo Hengyi Chemical Technology Co., Ltd. The polyethylene glycol (PEG) with a molar weight of 400, isobutanol (AR.), and HNO_3 (98 wt%) were purchased from Beijing Chemical Plant; deionized water was made in the lab.

The alumina catalyst modified by polyethylene glycol was prepared as follows. First, pseudo-boehmite powder (100 g) was mixed with Sesbania powder (2.3 g) with different proportions of PEG (10 g, 20 g, and 30 g, marked as 10%, 20%, and 30%) and even mixing. The mixture was then stirred vigorously for 30 min at 25 °C to form a homogeneous mixture. A 2 wt% dilute nitric acid solution was added to the mixture and mixed well. After mixing into a dough shape, we used a 3 mm diameter template for extrusion. The catalyst was dried at 25 °C for 12 h and then dried at 120 °C for 8 h, followed by calcination in air at 550 °C for 6 h to prepare the strip-shaped gamma-Al_2O_3 catalyst.

Table 3 Compressive strength of PEG-modified Al_2O_3 at different PEG loadings

Catalyst	Compressive strength N mm^{-1}
Al_2O_3	11.6
10% PEG-Al_2O_3	10.4
20% PEG-Al_2O_3	9.8
30% PEG-Al_2O_3	9.6

3.2. Catalytic reaction

The dehydration of isobutanol was performed in a fixed-bed down-flow stainless steel reactor with an inner diameter of 17 mm. Prior to the reaction, 15 mL of catalyst was placed in the catalyst bed and heated at 550 °C with an ambient pressure of N_2 for 2 h to activate the catalyst. After activation, isobutanol containing 5% water was used as the raw material. The raw material was fed through the top of the reactor at a liquid feed rate of 12 h^{-1}. The temperature was maintained at 330 °C and the pressure was 2 MPa. The product was divided into gas phase and liquid phase after passing through the condensing tank and the distributor tank. The liquid phase was collected every 2 h and analyzed by a FID-GC (GC-9790II, FL) with a 50 m × 0.53 mm capillary column of GS-ALUMINA (Agilent). The conversion and selectivity were calculated as follows:

$$\text{conversion } (\%) = \frac{\text{sum of moles of all products}}{\text{mole of the reactant}} \times 100, \quad (1)$$

$$\text{selectivity } (\%) = \frac{\text{moles of carbon in specific product}}{\text{moles of carbon in all products}} \times 100 \quad (2)$$

3.3. Characterization of the catalysts

The ammonia temperature programmed desorption (NH_3-TPD) technique was conducted by an Auto Chem II 2920 instrument (Micromeritics, USA) using a TCD detector. In the sample pretreatment stage, around 200 mg of sample was activated with Ar (99.999%) gas at a rate of 30 mL min^{-1} and 550 °C for 1 h. Prior to the experiment, NH_3 was adsorbed at 150 °C by flowing NH_3 (10%) at 40 mL min^{-1}. The TPD profile was obtained in the temperature range of 150–550 °C under Ar (99.999%).

The X-ray diffraction (XRD) measurements of the sample were performed with a Bruker spectrometer model D8 Advance using Cu Kα radiation (27.5 kV, 30 mA) with a wavelength of 0.01 nm.

The compressive strength of the samples was measured using a ZQJ-III intelligent particle strength testing machine (Shanghai Biao Science Instrument Co., Ltd).

The total pore volumes of the samples were measured using a Micromeritics AutoPore IV 9510 Mercury Intrusion Porosimeter (MIP). A mercury contact angle of 130° and a mercury interfacial tension of 485 dyne cm^{-1} were used to calculate the pore size distribution.

The specific surface area of the alumina solids was estimated from the adsorption–desorption isotherms of nitrogen at −196 °C, using Micromeritics equipment, model ASAP 2020, and previous degasification at 100 °C for 1 h.

The thermo gravimetry-differential thermal analysis (TG-DTA) was performed using a Thermoplus 8120 × 10^2 (Rigaku, Japan) under the following conditions: sample weight, *ca.* 5 mg; heating rate, 5 °C min^{-1}; heating range, from room temperature to 800 °C.

4. Conclusions

The pore structure of an activated alumina catalyst has a significant effect on the performance of isobutanol dehydration to isobutene. Adding polyethylene glycol during the preparation process of the activated alumina catalyst does not affect the crystal structure of the catalyst, can produce macropores and pore volume, improves the mass transfer performance of the catalyst, increases the conversion rate of isobutanol, and inhibits the superposition reaction of isobutylene. The conversion rate of isobutanol of the catalyst is continuously improved with increasing pore expander addition.

The isobutanol dehydration performance of the catalyst is better when 30% pore expander is added to the activated alumina catalyst. The compressive strength can meet the requirements of industrial applications. When the temperature is 330 °C, the pressure is 0.1 MPa, and the volume liquid space velocity is 12 h^{-1}. The conversion of isobutanol is maintained at about 97%, and the selectivity of isobutene is maintained at about 93% for 24 hours.

Funding

This research received no external funding.

Author contributions

Data acquisition and formal analysis, Zhao Yapeng; writing – original draft preparation, Tian Kaige and Li Qin; writing – review and editing, Tian Kaiege; methodology, Zhou Guanglin; supervision, Jiang Weili. All authors have read and agreed to the published version of the manuscript.

Conflicts of interest

The authors declare no conflict of interest.

References

1 V. Iannazzo, G. Neri, S. Galvagno, M. D. Serio, R. Tesser and E. Santacesaria, Oxidative dehydrogenation of isobutane over V2O5-based catalysts prepared by grafting vanadyl alkoxides on TiO2-SiO2 supports, *Appl. Catal., A*, 2003, **246**(1), 49–68.

2 G. S. Pozan, A. N. Tavman and I. Boz, Dehydroisomerization of n -butane over Cr/SiO 2, *Chem. Eng. J.*, 2008, **143**(1–3), 180–185.

3 G. Wang, C. Li and H. Shan, Highly Efficient Metal Sulfide Catalysts for Selective Dehydrogenation of Isobutane to Isobutene, *ACS Catal.*, 2014, **4**(4), 1139–1143.

4 M. E. Quiroga, N. S. Fígoli and U. A. Sedran, Synthesis of methyl tert-butyl ether on sulfur-promoted ZrO2, *Chem. Eng. J.*, 1997, **67**(3), 199–203.

5 D. I. Shiman, I. V. Vasilenko and S. V. Kostjuk, Cationic polymerization of isobutylene by AlCl3/ether complexes in non-polar solvents: Effect of ether structure on the selectivity of β-H elimination, *Polymer*, 2013, **54**(9), 2235–2242.

6 S. S. Jayadeokar and M. M. Sharma, Absorption of isobutylene in aqueous ethanol and mixed alcohols: cation exchange resins as catalyst, *Chem. Eng.*, 1992, **47**(13–14), 3777–3784.

7 D. H. Kim, D. G. Lee, J. K. Park, Y. H. Yang, J. K. Park and J. J. Yoon, A wood-rot fungus-mediated production of isobutylene from isobutanol, *Fuel*, 2019, **253**, 857–863.

8 D. S. Gogerty and T. A. Bobik, Formation of Isobutene from 3-Hydroxy-3-Methylbutyrate by Diphosphomevalonate Decarboxylase, *Appl. Environ. Microbiol.*, 2010, **76**(24), 8004–8010.

9 K. A. Tereshchenko and N. V. Ulitin, The Fundamental Kinetics of the Process of Butyl Rubber Synthesis, *Int. Polym. Sci. Technol.*, 2016, **43**(4), T27–T32.

10 I. U. A. Sangalov and G. E. Zaikov, *Polymers derived from isobutylene : synthesis, properties, application*. VSP: 2001.

11 E. B. H. Steiner, *Introduction to petroleum chemicals: based on lectures given at the Manchester College of Science and Technology*, 1961.

12 G. A. Olah and Á. Molnár, *Hydrocarbon Chemistry*, 2nd edn 2003.

13 V. C. Nelson, Introduction to Renewable Energy, *Appl. Mech. Rev.*, 2011, **61**(1), 129–137.

14 D. Gogerty *Isobutene formation from 3-hydroxy-3-methylbutyrate (3-HMB) by the Saccharomyces cerevisiae diphosphomevalonate decarboxylase (ScMDD) and directed enzyme evolution to improve enzyme function*, Iowa State University, 2011.

15 H. Fukuda, T. Fujii and T. Ogawa, Microbial Production of C3- and C4-Hydrocarbons under Aerobic Conditions, *J. Agric. Chem. Soc. Jpn.*, 1984, **48**(6), 1679–1682.

16 T. Fujii, T. Ogawa and H. Fukuda, Isobutene production byRhodotorula minuta, *Appl. Microbiol. Biotechnol.*, 1987, **25**(5), 430–433.

17 J. Becerra, E. Quiroga, E. Tello, M. Figueredo and M. Cobo, Kinetic modeling of polymer-grade ethylene production by diluted ethanol dehydration over H-ZSM-5 for industrial design, *Int. J. Chem. Environ. Eng.*, 2018, **6**(5), 6165–6174.

18 J. Bedia, R. Ruiz-Rosas, J. Rodríguez-Mirasol and T. Cordero, A kinetic study of 2-propanol dehydration on carbon acid catalysts, *J. Catal.*, 2010, **271**(1), 33–42.

19 T. K. Phung, A. Lagazzo, M. Á. R. Crespo, V. S. Escribano and G. Busca, A study of commercial transition aluminas and of their catalytic activity in the dehydration of ethanol, *J. Catal.*, 2014, **311**, 102–113.

20 J. D. Taylor, M. M. Jenni and M. W. Peters, Dehydration of Fermented Isobutanol for the Production of Renewable Chemicals and Fuels, *Top. Catal.*, 2010, **53**(15–18), 1224–1230.

21 D. V. Potapenko, L. Zhisheng and L. Yang, 2-Propanol reactivity on *in situ* prepared Au(1 1 1)-supported TiO2 nanocrystals, *J. Catal.*, 2013.

22 J. M. Müller, G. C. Mesquita, S. M. Franco, L. D. Borges and S. C. L. Dias, Solid-state dealumination of zeolites for use as

catalysts in alcohol dehydration, *Microporous Mesoporous Mater.*, 2015, **204**, 50–57.

23 K. Mori, H. Kakudo and H. Yamashita, Creation of Nickel-Based Active Species within a Macroreticular Acidic Resin: A Noble-Metal-Free Heterogeneous Catalyst for Visible-Light-Driven H2 Evolution from Water, *ACS Catal.*, 2014, **4**(11), 4129–4135.

24 R. L. Musante, R. J. Grau and M. A. Baltanás, Kinetic of liquid-phase reactions catalyzed by acidic resins: the formation of peracetic acid for vegetable oil epoxidation, *Appl. Catal., A*, 2000.

25 L. Shanshan, L. Ning, L. Guangyi, L. Lin, A. Wang, Y. Cong and W. Xiaodong, Lignosulfonate-based acidic resin for the synthesis of renewable diesel and jet fuel range alkanes with 2-methylfuran and furfural, *Green Chem.*, 2015.

26 N. Katada, K. Suzuki, T. Noda, G. Sastre and M. Niwa, Correlation between Brønsted Acid Strength and Local Structure in Zeolites, *J. Phys. Chem. C*, 2009.

27 L. Wang and F. S. Xiao, Nanoporous catalysts for biomass conversion, *Green Chem.*, 2015, **17**.

28 W. Z. Lang, C. L. Hu, L. F. Chu and Y. J. Guo, Hydrothermally prepared chromia-alumina (xCr/Al_2O_3) catalysts with hierarchical structure for propane dehydrogenation, *RSC Adv.*, 2014, **4**(70), 37107.

29 W. G. Adam, J. Sebastian, W. G. Adam, M. Barbara, K. T. Piotr and M. Piotr, Catalytic Behavior of Chromium Oxide Supported on Nanocasting-Prepared Mesoporous Alumina in Dehydrogenation of Propane, *Nanomaterials*, 2017, **7**(9), 249.

30 J. Wang; A. H. Lu; M. Li; W. Zhang; Y. S. Chen; D. X. Tian and W. C. Li, *Thin Porous Alumina Sheets as Supports for Stabilizing Gold Nanoparticles*. 2013.

31 W. Hai-zhi, S. Li-li, S. Zhi-jun, Z. Yi-an, Y. Guang-hua, C. De, Z. Xing-gui and Y. Wei-kang, Guang-Hua, Coke Formation on Pt-Sn/Al2O3 Catalyst for Propane Dehydrogenation, *Ind. Eng. Chem. Res.*, 2018.

32 Y. Wei, D. Jin, T. Ding, W. H. Shih and Q. Fu, A Non-surfactant Templating Route to Mesoporous Silica Materials, *Adv. Mater.*, 1998, **10**(4), 313–316.

33 J. Y. Zheng, J. B. Pang, K. Y. Qiu and Y. Wei, Synthesis and characterization of mesoporous titania and silica–titania materials by urea templated sol–gel reactions, *Microporous Mesoporous Mater.*, 2001, **49**(1–3), 189–195.

34 L. R. Pizzio, Mesoporous titania: effect of thermal treatment on the texture and acidic properties, *Mater. Lett.*, 2005, **59**(8/9), 994–997.

35 Y. Zhang, Y. Zhou, A. Qiu, Y. Wang, Y. Xu and P. Wu, Effect of Alumina Binder on Catalytic Performance of PtSnNa/ZSM-5 Catalyst for Propane Dehydrogenation, *Ind. Eng. Chem. Res.*, 2006, **45**(7), 2213–2219.

36 L. Osiglio, G. Sathicq, L. Pizzio, G. Romanelli and M. Blanco, Preparation of acetates catalyzed by boric acid and/or tungstophosphoric acid-modified zirconia obtained employing polyethylene glycols as pore-forming agents, *J. Mol. Catal. Chem.*, 2016, S1381116916304605.

37 X. Q. Gao, W. D. Lu, S. Z. Hu, W. C. Li and A. H. Lu, Rod-shaped porous alumina-supported Cr2O3 catalyst with low acidity for propane dehydrogenation, *Chin. J. Catal.*, 2019, **40**(2), 184–191.

38 Z. Zhang, Y. Wang, K. Sun, Y. Shao, L. Zhang, S. Zhang, X. Zhang, Q. Liu, Z. Chen and X. Hu, Steam reforming of acetic acid over Ni-Ba/Al_2O_3 catalysts:Impacts of barium addition on coking behaviors and formation of reaction intermediates, *J. Energy Chem.*, 2020, **43**(04), 208–219.

39 F. Geobaldo, G. Spoto, S. Bordiga, C. Lamberti and A. Zecchina, Propene oligomerization on H-mordenite: Hydrogen-bonding interaction, chain initiation, propagation and hydrogen transfer studied by temperature-programmed FTIR and UV–VIS spectroscopies, *J. Chem. Soc., Faraday Trans.*, 1997, **93**(6), 1243–1249.

40 A. Travert, T. Onfroy, G. Clet, A. Aboulayt and F. Mauge, Relationship between phosphate structure and acid-base properties of phosphate-modified zirconia-Application to alcohol dehydration, *Appl. Catal., A*, 2017.

41 A. Gervasini, G. Bellussi, J. Fenyvesi and A. Auroux, Microcalorimetric and Catalytic Studies of the Acidic Character of Modified Metal Oxide Surfaces. 1. Doping Ions on Alumina, Magnesia, and Silica, *J. Phys. Chem.*, 1995, **99**(14), 5117–5125.

42 Y. W. Sun, Y. J. Wang, W. Guo, T. Wang and G. S. Luo, Triblock copolymer and poly(ethylene glycol) as templates for monolithic silica material with bimodal pore structure, *Microporous Mesoporous Mater.*, 2006, **88**(1–3), 31–37.